SAND2018-1266J

Letter

Cite This: *ACS Photonics* XXXX, XXX, XXX−XXX

Enhanced Second-Harmonic Generation Using Broken Symmetry III−V Semiconductor Fano Metasurfaces

Polina P. Vabishchevich,*[,†,‡] Sheng Liu,[†,‡] Michael B. Sinclair,[†] Gordon A. Keeler,[†] Gregory M. Peake,[†] and Igal Brener*[,†,‡]

[†]Sandia National Laboratories, Albuquerque, New Mexico 87185, United States

[‡]Center for Integrated Nanotechnologies, Sandia National Laboratories, Albuquerque, New Mexico 87185, United States

Supporting Information

ABSTRACT: All-dielectric metasurfaces, two-dimensional arrays of subwavelength low loss dielectric inclusions, can be used not only to control the amplitude and phase of optical beams, but also to generate new wavelengths through enhanced nonlinear optical processes that are free from some of the constraints dictated by the use of bulk materials. Recently, high quality factor (Q) resonances in these metasurfaces have been revealed and utilized for applications such as sensing and lasing. The origin of these resonances stems from the interference of two nanoresonator modes with vastly different Q. Here we show that nonlinear optical processes can be further enhanced by utilizing these high-Q resonances in broken symmetry all-dielectric metasurfaces. We study second harmonic generation from broken symmetry metasurfaces made from III−V semiconductors and observe nontrivial spectral shaping of second-harmonic and multifold efficiency enhancement induced by high field localization and enhancement inside the nanoresonators.

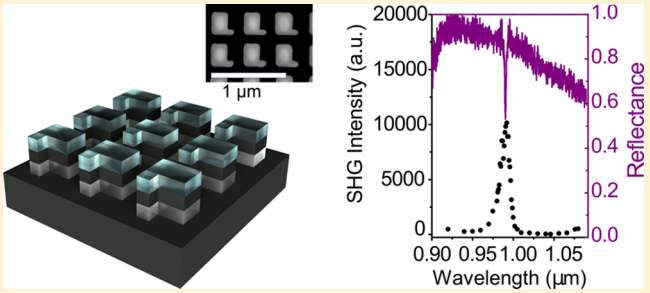

KEYWORDS: *second-harmonic generation, dielectric metasurfaces, Fano resonances, III−V semiconductors*

Frequency conversion such as harmonic generation, is one of the most fundamental manifestations of the nonlinear optical response of materials.[1,2] This phenomenon has had profound impact in multiple applications that have affected our daily life, from manufacturing, to energy, displays and scientific research. Nonlinear frequency conversion requires the use of a macroscopic amount of a nonlinear material. The use of such bulk media in small devices remains challenging: the intrinsic nonlinearities in materials are extremely weak, and efficient harmonic generation can be achieved either with long interaction lengths or with strong field intensities. Moreover, nonlinear processes require careful matching of the optical phases of the fundamental beams and the newly generated frequencies. Artificially structured materials, such as metamaterials, plasmonic nanostructures, or metasurfaces, allow us to overcome some or all of these constraints, paving the way for a new wave of revolutionary concepts and devices that will enable more efficient and flexible harmonic generation or frequency mixing.[3,4]

The need for optical phase matching is a direct consequence of using materials that are many orders of magnitude thicker than the wavelength of light. Highly nonlinear, subwavelength, and thin nanostructured materials either relax or eliminate the need for phase matching between any of the beams involved in the optical mixing process.[5] Moreover, their nanoscale dimensions and mode structure often lead to tight confinement and resonant enhancement of electromagnetic fields, giving rise to a multifold increase in frequency conversion efficiencies. For example, in the past ∼35 years, surface plasmons or localized plasmonic excitations have been widely employed in optical frequency mixing, providing enhanced nonlinear effects with ultrafast response times.[6] However, due to the relatively small damage threshold of plasmonic structures, achieving high conversion efficiencies in pure metallic nanostructures is fundamentally difficult. One potential path to overcoming these limitations relies on the use of high-index dielectric nanoparticles or metasurfaces that support the excitation of Mie modes.[7,8] In contrast to plasmonic nanostructures, the electromagnetic field is confined inside the nanoparticle, leading to a more efficient use of the bulk nonlinearity. Also, different materials with a wide spectrum of optical nonlinearities and tensor symmetries can be used in an all-dielectric approach. For example, metasurfaces made from III−V semiconductors with large intrinsic second-order nonlinearities exhibit strong second-harmonic generation (SHG) induced by the tight electromagnetic field confinement inside the nanoresonators.[9−13] Third-order nonlinear processes, such as third-harmonic generation (THG) and four-wave mixing in Si and

Special Issue: Ultra-Capacity Metasurfaces with Low Dimension and High Efficiency

Received: December 4, 2017
Published: January 27, 2018

DOI: 10.1021/acsphotonics.7b01478
ACS Photonics XXXX, XXX, XXX−XXX

Ge metasurfaces, have also been reported recently.[14−19] Finally, the implementation of Mie-type localized modes with high quality factor resonances, that is, Fano resonances, have led to the highest values of conversion efficiencies in nanostructures reported so far.[20,21] Typically, a Fano resonance arises due to the interference between a broad scattering channel and a resonant one.[22−25] The constructive and destructive interference of these channels results in an asymmetric dip and/or peak in the transmittance/reflectance spectrum with high-Q factors. For example, the interference between the highly resonant dark mode of a Si nanodisc, with the bright mode of a Si slit, led to a Fano resonance with $Q \sim 466$; these structures were used for high-efficiency third harmonic generation.[20] Another design that supports a Fano-resonant mode leading to THG enhancement consists of quadromers of high-index nanoresonators.[21,26,27]

Recently, we reported on a new paradigm for creating record high $Q \sim 600$ resonances in all-dielectric metasurfaces using a broken symmetry design to couple radiating modes with symmetry protected dark modes.[28] These designs provide a more robust and simple alternative for creating high-Q Fano resonances with arrays of nanoscaled dimensions. Here we demonstrate the enhanced generation of second harmonic (SH) in such a broken symmetry GaAs-based metasurface, that contains Mie-typed localized modes with high-Q factor Fano resonances. The strongly enhanced local fields inside the nanoresonators lead to multifold enhancement of the second-harmonic signal. Our results have important implications for novel nonlinear optical devices since further improvements are possible both in the nanoresonators designs and the choice of constituent material with a more favorable nonlinear tensor.

RESULTS AND DISCUSSION

The schematic of the Fano-resonant metasurface is shown in Figure 1a; it consists of an array of broken symmetry nanoresonators. The design is based on a small cube with a side of ∼300 nm, that has a notch cut from its corner. The Fano metasurfaces were fabricated using a recently published procedure[9] that involves mask-etching of GaAs/AlGaAs heterostructures, and subsequent oxidation of an AlGaAs layer to AlGaO (see Supporting Information). Insets in Figure 1a show a top-view and a 20° side-view scanning electron microscope (SEM) images of the fabricated metasurface consisting of an array of broken symmetry nanoresonators with ∼470 nm pitch. The dimensions of the structure were chosen to scale the Fano resonance to a wavelength longer than the GaAs bandgap to avoid absorption of the pump. This shape of the nanoresonator leads to mode mixing between the transverse and longitudinal dipole modes for normal incidence light, which results in a Fano resonance with high-Q values.[28] These resonances can be observed both in transmission or reflection spectra.

We characterized the metasurface sample with measurements of the linear spectra using a custom-made setup for micro-reflectance. Light from a white light source was focused by a 10× Mitutoyo Plan Apo NIR objective with 0.26 Numerical Aperture (NA) and the reflected signal was collected through the same objective. The reflectance spectra of the metasurface, normalized to a silver mirror response is shown in Figure 1b. The high-reflectance spectral region, starting from 0.92 μm, corresponds to the excitation of Electric Dipole (ED) and Magnetic Dipole (MD) Mie modes as verified by finite-difference time-domain (FDTD) calculations using FDTD

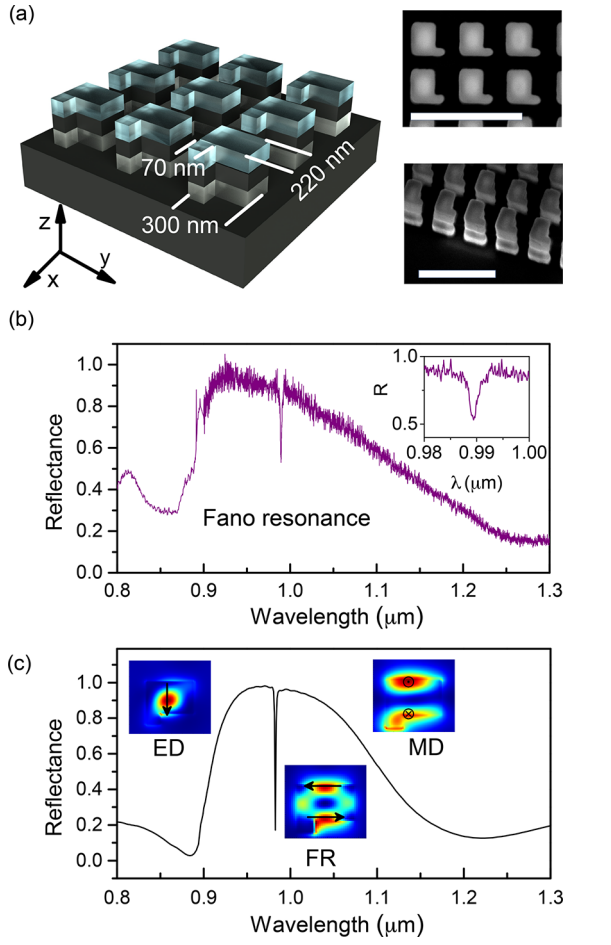

Figure 1. Symmetry broken GaAs metasurface used to create high-Q Fano resonances. (a) Schematic of a Fano-resonant metasurface design, based on a cube with a ∼300 nm side that has a notch cut from the corner. Inset top: a top-view SEM image of the fabricated Fano metasurface. Inset bottom: a 20° side-view SEM image of the fabricated Fano metasurface. The scale bar corresponds to 1 μm. (b) Reflectivity spectrum of the Fano metasurface, that exhibits a high-Q resonance with a ∼2 nm spectral width. Inset is a zoomed in region of the reflectivity spectrum around the Fano resonance. (c) Simulated reflectance spectra with electric field intensity profiles, corresponding to the maxima of field enhancement of Fano resonance, the ED and the MD resonances in the horizontal $x-y$ plane located half way through the GaAs nanoresonator. Arrows indicate the directions of electromagnetic field vectors inside the nanoresonator at peak intensities.

Solutions by Lumerical Solutions, Inc. Figure 1c shows cross sections of electric field maps, calculated for a horizontal $x-y$ plane located half way through the GaAs nanoresonators. The electric field strength undergoes a 7-fold enhancement inside the resonator for a wavelength corresponding to the MD resonance ($\lambda_{MD} \sim 1.097$ μm). The sharp dip in the reflectance spectra in Figure 1b at $\lambda_F \sim 0.99$ μm corresponds to the excitation of the Fano resonance with a spectral width of $\Delta\lambda \sim 2$ nm (Q factor $\lambda_F/\Delta\lambda \sim 500$). Note that the measured full width at half-maximum (fwhm) of the Fano resonance strongly depends on the NA of the objective used, since the resonance spectral position is sensitive to the light incident angle. The local map of the electric field inside the nanoresonator for a wavelength corresponding to the Fano resonance shows an in-plane circulating structure (Figure 1c). The magnetic field for

DOI: 10.1021/acsphotonics.7b01478
ACS Photonics XXXX, XXX, XXX−XXX

excitation at the Fano resonance is oriented out-of-plane showing the efficient excitation of the symmetry protected out-of-plane magnetic dipole mode; see Supporting Information. Numerical calculations show that in the ideal nanostructure, the enhancement of the electric field inside the nanoresonator at the Fano resonance reaches a value of $|E|^2/|E_0|^2 \sim 500$. This is almost 2 orders of magnitude higher than the intensity values at the transverse MD resonance for this structure.

In our harmonic generation experiments we expect the SHG signal to be at wavelengths shorter than the GaAs band gap (~860 nm at room temperature), thus, absorbed by the substrate. Therefore, we used a reflectance geometry to measure the nonlinear response from the metasurface. In the experimental setup, we used a tunable mode-locked Ti:sapphire laser oscillator that produced 130 fs laser pulses at 80 MHz repetition rate; for further details, see Supporting Information. Figure 2 shows the intensity of the second harmonic signal generated by the GaAs broken symmetry metasurface when the pump power was kept constant and the pump wavelength was swept across the Fano resonance. The SHG intensity spectrum exhibits a narrow peak at ~0.99 μm with a fwhm of ~14 nm that corresponds to the position of the Fano resonance in the linear spectrum (also shown in Figure 2). Due to the electromagnetic field localization and increase of its intensity inside the nanoresonator occurring for the Fano-resonant wavelength, the SHG signal when the pump laser is tuned to the Fano resonance is ~300× stronger compared to the off-resonant case. The small rise of the SHG intensity at longer wavelengths (>1.05 μm) is likely caused by the excitation of the broad transverse MD resonance that peaks at a wavelength beyond the tunable range of our laser. The weak increase of the SHG signal at shorter wavelengths (<0.95 μm) is caused by the excitation of the broad transverse ED resonance.

Because the spectral width of the short pulse pump used in our experiments ($\Delta\lambda_{pulse} \sim 11$ nm) exceeds the spectral width of the sharp Fano resonance ($\Delta\lambda_F \sim 2$ nm), the pump spectrum and SHG spectral response have to be accounted for carefully. Figure 3a shows the scenario of the modification of a normalized SHG spectrum when the pump carrier wavelength is detuned from the resonant wavelength covering a detuning from −10 to +20 nm. When $\Delta\lambda = -10$ nm, there is no overlap with the Fano resonance and the shape of the generated second harmonic is close to Gaussian. As the detuning becomes smaller, from −9 to −3 nm, the longer wavelength part of the pump pulse starts to couple to the Fano resonance. Thereby, a two-peak structure of the generated SH appears: longer wavelengths of the SHG are enhanced more than shorter wavelengths. This leads to a slight shift of the SHG peak intensity wavelength from the expected doubled frequency. When the central wavelength of the pump pulse overlaps with the dip of the Fano resonance, the central portion of the pump pulse is coupled with the sharp Fano resonance, and the generated SH spectrum becomes narrower. Further detuning from the resonant wavelength leads to the reverse behavior of the SHG spectral shape—the shorter wavelengths of SHG are enhanced more, leading to a double peak shape of the SH spectrum.

Figure 3b shows a comparison between the SH spectrum obtained from the GaAs metasurface when pumping at the Fano-resonant wavelength and the SH generated from the unpatterned region of the GaAs substrate. First and as mentioned earlier, the SH spectral shape is slightly modified; its spectral width is narrowed down to ~2.3 nm, which is less than the spectral width of the SH generated by the substrate (~3.5 nm). Moreover, the intensity of the SH signal when pumping exactly at the Fano resonance is more than 4 orders of magnitude higher than the SH signal obtained from the unpatterned GaAs.

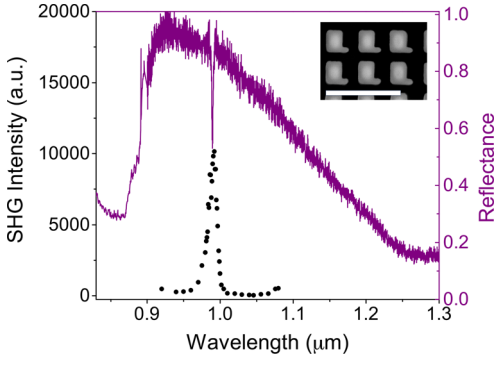

Figure 2. Second harmonic generation (SHG) from the Fano resonance metasurface. Dots: experimental spectral dependence of the SHG intensity showing resonantly enhanced SHG at the Fano resonance wavelengths. Purple: linear reflectivity spectrum of the Fano metasurface. Inset: a top-view SEM image of the sample.

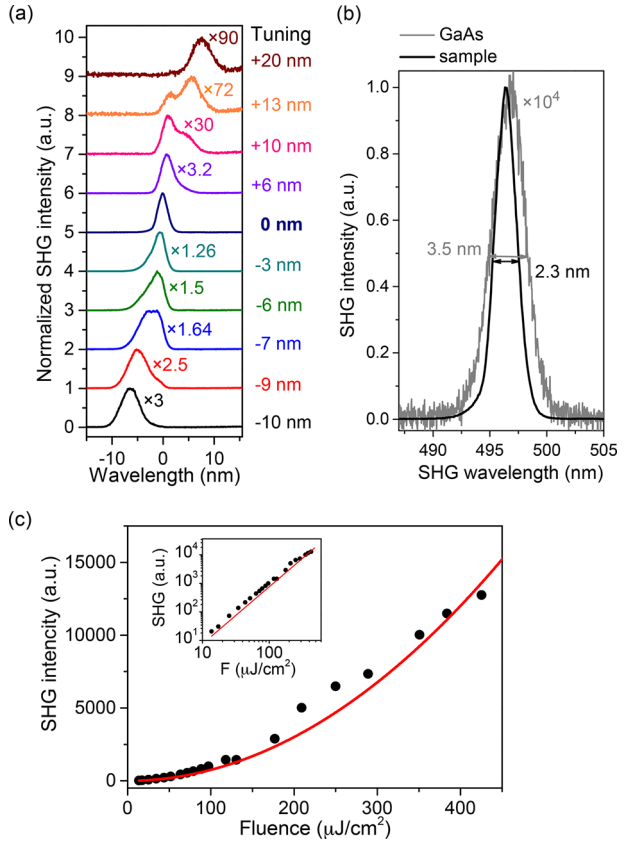

Figure 3. (a) Modification of the normalized SHG spectrum when the pump carrier wavelength is detuned from the Fano-resonant wavelength, from −10 to +20 nm. Strong electromagnetic field coupling only at the Fano resonance wavelength leads to the appearance of a second peak in the SH spectra. (b) Narrowing of the spectra of the SH generated by the Fano metasurface (black line) in comparison with SH generated by the unpatterned GaAs substrate (gray line). (c) Power dependence of the SH intensity plotted against the pump fluence. Red line shows a quadratic fit.

DOI: 10.1021/acsphotonics.7b01478
ACS Photonics XXXX, XXX, XXX−XXX

To confirm the generation mechanism of the detected signal, we performed measurements of SH intensity when pumping at the Fano resonance as a function of the incident pump fluence. The measured integrated SH signal shows a quadratic dependence on the incident power. However, after reaching a fluence of 400 μJ/cm^2, the generated SH starts to saturate and further increase of the pump power leads to irreversible damage of the sample. Moreover, when the pump center wavelength is slightly detuned from the resonance, the damage occurs at higher fluencies as less incident power is coupled to the nanoresonator. The damage is most likely caused by two-photon absorption induced thermal heating, enhanced by the high field energy density concentrated inside the nanoresonator.

Recent experimental observations of SHG from dielectric metasurfaces that rely on Mie resonances[9] show a maximum conversion efficiency of $\sim 2 \times 10^{-5}$. In order to compare the overall performance of the broken symmetry metasurface, we compared the SH signals to that measured from a metasurface consisting of GaAs nanodiscs; the latter was the same sample used in ref 9. The GaAs nanodiscs have a diameter of 250 nm and height of 300 nm, arranged into an array with a pitch of 600 nm; a SEM micrograph of such array is shown in the inset of Figure 4a.

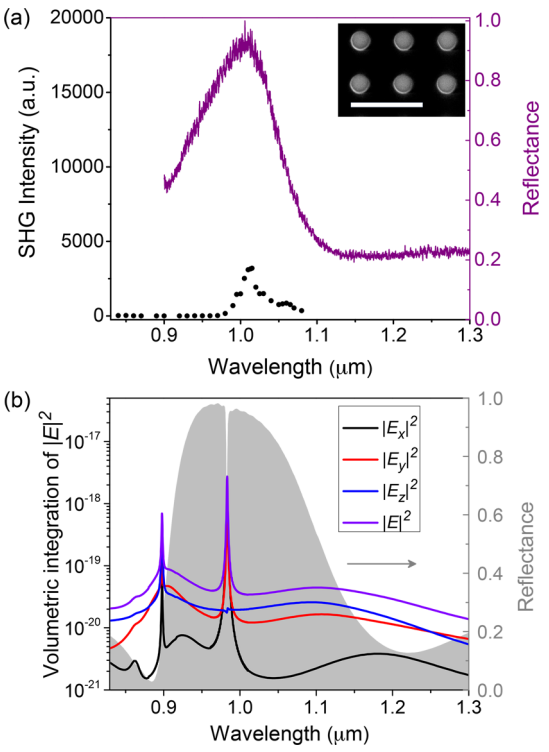

Figure 4. SHG from the Fano resonance metasurface in comparison with SH generated by a nanodisc sample. (a) Purple line: reflectivity spectrum of the nanodisc metasurface. Dots: experimental results of the SHG intensity spectrum, showing the resonantly enhanced SHG at the magnetic dipole resonance wavelength of a nanodisc. Top inset: a top-view SEM image of a nanodisc metasurface sample. The scale bar corresponds to 1 μm. (b) Results of numerical FDTD calculations. The squared magnitude of the electric field integrated over the volume of the resonator shows a multifold enhancement at the Fano resonance wavelengths. Different components are depicted by a different color. The calculated linear reflectivity spectrum of the Fano metasurface is used as a gray-shaded background.

The linear reflectivity spectra of the symmetric nanodisc metasurface, as well as the spectral dependence of its SH intensity measured with the same pump-power as in the Fano metasurface case, exhibit a peak at a wavelength of $\sim$1 μm, which corresponds to the MD resonance. It is clearly seen that the maximum SHG efficiency for the Fano metasurface is three times higher than the maximum efficiency for the nanodisc metasurface sample. Another noticeable difference is that the spectral width of the enhanced spectral region in the case of the nanodisc resonance is wider, due to the low Q factor of the transverse magnetic dipole resonance.

It is well-known, that the total nonlinear polarization of the GaAs metasurface is influenced by several factors. One of them is the enhancement of the electromagnetic field inside the nanoresonator that influences directly the conversion efficiency of the nonlinear process. To clarify the experimental results, we performed numerical calculations of volume integrated local electromagnetic fields within the nanoresonators. First, we retrieved all three electric field components, $E_i(\mathbf{r}, \lambda)$, within the nanoresonators arranged into a square array. Local field maps were integrated over the resonator volume for each wavelength. The spectra of the squared field magnitude for the different spatial components are shown in Figure 4b. First, two broad Mie-resonant contributions can be seen with maxima at $\sim$1.1 μm for the MD resonance and at $\sim$0.9 μm for the ED resonance. Furthermore, the two distinct and narrow features shown in Figure 4b that have the largest electromagnetic fields values, correspond to the excitation of the symmetry protected vertical dipole modes. One of them is the out-of-plane MD resonance at $\sim$0.98 μm, the same one we utilized for the SHG enhancement. The total electromagnetic field inside the nanoresonator at the resonant Fano wavelength is a few orders of magnitude higher than for the broad MD resonance; this additional field enhancement is responsible for the higher SHG efficiency when pumping at the Fano resonance wavelength. More importantly, a comparison of the electric field components in Figure 4b reveals that almost only E_x and E_y contribute to the total field inside the nanoresonator. On the other hand, for the high-Q resonance at $\sim$0.9 μm, high values of electric field can be seen only for the z-component, because the electric field inside the nanoresonator in this case is directed out-of-plane. Note that since the Q of the out-of-plane electric dipole mode is higher than for the out-of-plane magnetic dipole mode and its resonance wavelength lies at a region of low reflectance, it was almost impossible to distinguish its presence in the reflectance spectra as shown in gray in Figure 4b.

Due to the zinc blende crystalline structure of GaAs, the nonlinear susceptibility tensor for the bulk material contains only off-diagonal components $\chi^{(2)}_{ijk}$ with $i \neq j \neq k$, where i, j, k, represent spatial coordinates x, y, z. Thereby, the ith component of the nonlinear polarization vector inside the [100] oriented GaAs for SHG is $P_i^{(2\omega)} \propto \chi^{(2)}_{ijk} E_j^{(\omega)} E_k^{(\omega)}$. However, for example, for the ED-based Fano resonance at $\sim$0.9 μm, only the z-component of the electric field is enhanced. In this case, higher nonlinear polarization values can be expected for [110] GaAs, where the nonlinear polarization is given by $P_i^{(2\omega)} \propto \chi^{(2)}_{ij} E_j^{(\omega)} E_j^{(\omega)}$. Another important factor that should be taken into the account is related to the intrinsic material properties of GaAs. Due to the symmetry broken design, the excitation of the Fano resonances is sensitive to the incident light polarization state. So is the SHG in the bulk GaAs. Therefore, to optimize the SHG in the Fano metasurfaces, it might be necessary to match the asymmetric shape of the sample with the crystalline

DOI: 10.1021/acsphotonics.7b01478
ACS Photonics XXXX, XXX, XXX−XXX

axis of the GaAs substrate; see Supporting Information. Nonetheless, a comprehensive study of these effects lies beyond the scope of this paper, since other contributions to the nonlinear susceptibility such as surface nonlinearities,[9] should be considered.

In this paper we show that the electric field enhancement in high-Q Fano metasurfaces at the fundamental frequency leads to ~3× higher SHG conversion efficiencies in comparison with nanodisc metasurface samples. In the SHG process it is also important to consider the spectral width of the pumping laser. Our experiment was performed with laser pulses with a spectral width of ~11 nm that is much larger than the line width of the Fano resonance (~2 nm); hence, less than 30% of the pump pulse was coupling to the metasurface resonance. Therefore, we can compare the obtained SHG intensity for the Fano metasurface with the SH generated by the nanodisc metasurface when it was pumped by the 3.3-times lower intensity pump. However, the Fano resonance metasurface has ~2.3× larger filling factor than the nanodisc sample, since the Fano nanoresonator array has a smaller array pitch than the nanodisc sample. Thereby, taking into consideration the facts stated above, we could achieve a ~13-fold enhancement of SHG by the Fano metasurface. Note that we are not taking into account the difference of the far-field emission profiles between the two metasurfaces, which can impact the estimation of conversion efficiencies, especially considering the low NA objective used. Another possibility to reach higher values of generated SH is to optimize the proposed design for longer wavelengths by enlarging the dimensions of the sample. First, a larger size of the cube will shift the Mie resonances, the Fano resonances, and the SH wavelengths below the GaAs bandgap, thus avoiding the reabsorption of the newly generated harmonic signals by the nanoresonator material. Finally, this scaling approach would allow us to utilize higher-order Mie resonances to achieve simultaneous field enhancement not only at the fundamental wavelengths, but also at the SH wavelengths.

To summarize, we have demonstrated visible narrow bandwidth SHG by utilizing a Fano resonance metasurface consisting of broken symmetry resonators. The use of Fano resonances allows us to achieve multifold enhancement of SHG in comparison with a GaAs nanodisc metasurface due to the high field confinement inside the Fano resonance nanostructure. The SHG process does not require any phase matching and the Fano metasurface exhibits a higher damage threshold compared to plasmonic metasurfaces or nanostructures. We expect that our design can be optimized further for more complex frequency conversion processes, and will open a new route toward realization of new metasurface-based optical devices.

■ ASSOCIATED CONTENT

Supporting Information

The Supporting Information is available free of charge on the ACS Publications website at DOI: 10.1021/acsphotonics.7b01478.

Detailed numerical calculations of electric fields inside the nanoresonators, descriptions of the fabrication process of the metasurfaces, the experimental SHG setup, measured SHG efficiency, and the polarization dependence of SHG (PDF).

■ AUTHOR INFORMATION

Corresponding Authors

*E-mail: pvabish@sandia.gov.
*E-mail: ibrener@sandia.gov.

ORCID

Polina P. Vabishchevich: 0000-0003-0795-2314
Igal Brener: 0000-0002-2139-5182

Notes

The authors declare no competing financial interest.

■ ACKNOWLEDGMENTS

This work was supported by the U.S. Department of Energy, Office of Basic Energy Sciences, Division of Materials Sciences and Engineering and performed, in part, at the Center for Integrated Nanotechnologies, an Office of Science User Facility operated for the U.S. Department of Energy (DOE) Office of Science. Sandia National Laboratories is a multi mission laboratory managed and operated by National Technology and Engineering Solutions of Sandia, LLC, a wholly owned subsidiary of Honeywell International, Inc., for the U.S. Department of Energy's National Nuclear Security Administration under contract DE-NA0003525.

■ REFERENCES

(1) Shen, Y.-R. *The Principles of Nonlinear Optics*; Wiley-Interscience: New York, 1984; p 575.
(2) Boyd, R. W. *Nonlinear Opt.*; Academic Press, 2003.
(3) Lapine, M.; Shadrivov, I. V.; Kivshar, Y. S. Nonlinear Metamaterials. *Rev. Mod. Phys.* **2014**, *86* (3), 1093−1123.
(4) Li, G.; Zhang, S.; Zentgraf, T. *Nonlinear Photonic Metasurfaces* **2017**, *2*, 17010.
(5) Krasnok, A.; Tymchenko, M.; Alù, A. Nonlinear Metasurfaces: a Paradigm Shift in Nonlinear Optics. *Mater. Today* **2017**, na.
(6) Kauranen, M.; Zayats, A. V. Nonlinear Plasmonics. *Nat. Photonics* **2012**, *6*, 737.
(7) Kuznetsov, A. I.; Miroshnichenko, A. E.; Fu, Y. H.; Zhang, J.; Luk'yanchuk, B. Magnetic Light. *Sci. Rep.* **2012**, *2* (7), 492.
(8) Kuznetsov, A. I.; Miroshnichenko, A. E.; Brongersma, M. L.; Kivshar, Y. S.; Luk'yanchuk, B. Optically Resonant Dielectric Nanostructures. *Science* **2016**, *354* (6314), 2472.
(9) Liu, S.; Sinclair, M. B.; Saravi, S.; Keeler, G. A.; Yang, Y.; Reno, J.; Peake, G. M.; Setzpfandt, F.; Staude, I.; Pertsch, T.; Brener, I. Resonantly Enhanced Second-Harmonic Generation Using III−V Semiconductor All-Dielectric Metasurfaces. *Nano Lett.* **2016**, *16* (9), 5426−5432.
(10) Camacho-Morales, R.; Rahmani, M.; Kruk, S.; Wang, L.; Xu, L.; Smirnova, D. A.; Solntsev, A. S.; Miroshnichenko, A.; Tan, H. H.; Karouta, F.; Naureen, S.; Vora, K.; Carletti, L.; De Angelis, C.; Jagadish, C.; Kivshar, Y. S.; Neshev, D. N. Nonlinear Generation of Vector Beams From AlGaAs Nanoantennas. *Nano Lett.* **2016**, *16* (11), 7191−7197.
(11) Gili, V. F.; Carletti, L.; Locatelli, A.; Rocco, D.; Finazzi, M.; Ghirardini, L.; Favero, I.; Gomez, C.; Lemaître, A.; Celebrano, M.; De Angelis, C.; Leo, G. Monolithic AlGaAs Second-Harmonic Nanoantennas. *Opt. Express* **2016**, *24* (14), 15965−15971.
(12) Kruk, S.; Camacho-Morales, R.; Xu, L.; Rahmani, M.; Smirnova, D. A.; Wang, L.; Tan, H. H.; Jagadish, C.; Neshev, D. N.; Kivshar, Y. S. Nonlinear Optical Magnetism Revealed by Second-Harmonic Generation in Nanoantennas. *Nano Lett.* **2017**, *17*, 3914.
(13) Liu, S.; Keeler, G. A.; Reno, J. L.; Sinclair, M. B.; Brener, I. III−V Semiconductor Nanoresonators—a New Strategy for Passive, Active, and Nonlinear All-Dielectric Metamaterials. *Adv. Opt. Mater.* **2016**, *4* (10), 1457−1462.
(14) Shcherbakov, M. R.; Neshev, D. N.; Hopkins, B.; Shorokhov, A. S.; Staude, I.; Melik-Gaykazyan, E. V.; Decker, M.; Ezhov, A. A.;

DOI: 10.1021/acsphotonics.7b01478
ACS Photonics XXXX, XXX, XXX−XXX

Miroshnichenko, A. E.; Brener, I.; Fedyanin, A. A.; Kivshar, Y. S. Enhanced Third-Harmonic Generation in Silicon Nanoparticles Driven by Magnetic Response. *Nano Lett.* **2014**, *14* (11), 6488−6492.
(15) Grinblat, G.; Li, Y.; Nielsen, M. P.; Oulton, R. F.; Maier, S. A. Efficient Third Harmonic Generation and Nonlinear Subwavelength Imaging at a Higher-Order Anapole Mode in a Single Germanium Nanodisk. *ACS Nano* **2017**, *11* (1), 953−960.
(16) Grinblat, G.; Li, Y.; Nielsen, M. P.; Oulton, R. F.; Maier, S. A. Degenerate Four-Wave Mixing in a Multiresonant Germanium Nanodisk. *ACS Photonics* **2017**, *4* (9), 2144−2149.
(17) Shcherbakov, M. R.; Werner, K.; Fan, Z.; Talisa, N.; Chowdhury, E.; Shvets, G. Non-Integer Harmonics Generation by Photon Acceleration in Rapidly Evolving Nonlinear Semiconductor Metasurfaces. *arXiv preprint arXiv:1710.06966* **2017**, na.
(18) Melik-Gaykazyan, E. V.; Shcherbakov, M. R.; Shorokhov, A. S.; Staude, I.; Brener, I.; Neshev, D. N.; Kivshar, Y. S.; Fedyanin, A. A. Third-Harmonic Generation From Mie-Type Resonances of Isolated All-Dielectric Nanoparticles. *Philos. Trans. R. Soc., A* **2017**, *375*, 20160281.
(19) Liu, S.; Vabishchevich, P. P.; Vaskin, A.; Reno, J. L.; Keeler, G. A.; Sinclair, M. B.; Staude, I.; Brener, I. An Optical Metamixer. *arXiv preprint arXiv:1711.00090* **2017**, na.
(20) Yang, Y.; Wang, W.; Boulesbaa, A.; Kravchenko, I. I.; Briggs, D. P.; Puretzky, A.; Geohegan, D.; Valentine, J. Nonlinear Fano-Resonant Dielectric Metasurfaces. *Nano Lett.* **2015**, *15* (11), 7388−7393.
(21) Shorokhov, A. S.; Melik-Gaykazyan, E. V.; Smirnova, D. A.; Hopkins, B.; Chong, K. E.; Choi, D.-Y.; Shcherbakov, M. R.; Miroshnichenko, A. E.; Neshev, D. N.; Fedyanin, A. A.; Kivshar, Y. S. Multifold Enhancement of Third-Harmonic Generation in Dielectric Nanoparticles Driven by Magnetic Fano Resonances. *Nano Lett.* **2016**, *16* (8), 4857−4861.
(22) Miroshnichenko, A. E.; Flach, S.; Kivshar, Y. S. Fano Resonances in Nanoscale Structures. *Rev. Mod. Phys.* **2010**, *82* (3), 2257.
(23) Fan, P.; Yu, Z.; Fan, S.; Brongersma, M. L. Optical Fano Resonance of an Individual Semiconductor Nanostructure. *Nat. Mater.* **2014**, *13* (5), 471−475.
(24) Luk'yanchuk, B.; Zheludev, N. I.; Maier, S. A.; Halas, N. J.; Nordlander, P.; Giessen, H.; Chong, C. T. The Fano Resonance in Plasmonic Nanostructures and Metamaterials. *Nat. Mater.* **2010**, *9* (9), 707−715.
(25) Wu, C.; Arju, N.; Kelp, G.; Fan, J. A.; Dominguez, J.; Gonzales, E.; Tutuc, E.; Brener, I.; Shvets, G. Spectrally Selective Chiral Silicon Metasurfaces Based on Infrared Fano Resonances. *Nat. Commun.* **2014**, *5*, 10.
(26) Miroshnichenko, A. E.; Kivshar, Y. S. Fano Resonances in All-Dielectric Oligomers. *Nano Lett.* **2012**, *12* (12), 6459−6463.
(27) Chong, K. E.; Hopkins, B.; Staude, I.; Miroshnichenko, A. E.; Dominguez, J.; Decker, M.; Neshev, D. N.; Brener, I.; Kivshar, Y. S. Observation of Fano Resonances in All-Dielectric Nanoparticle Oligomers. *Small* **2014**, *10* (10), 1985−1990.
(28) Campione, S.; Liu, S.; Basilio, L. I.; Warne, L. K.; Langston, W. L.; Luk, T. S.; Wendt, J. R.; Reno, J. L.; Keeler, G. A.; Brener, I.; Sinclair, M. B. Broken Symmetry Dielectric Resonators for High Quality Factor Fano Metasurfaces. *ACS Photonics* **2016**, *3* (12), 2362−2367.

DOI: 10.1021/acsphotonics.7b01478
ACS Photonics XXXX, XXX, XXX−XXX